JoT JOURNAL OF TURBULENCE

http://jot.iop.org/

Comparison between an experimental turbulent vortex and the Lundgren vortex

Yannis Cuypers[1], **Agnès Maurel**[2] and **Philippe Petitjeans**[1]

[1] Laboratoire de Physique et de Mécanique des Milieux Hétérogènes, Ecole Supérieure de Physique et de Chimie Industrielles, 10 rue Vauquelin, 75005 Paris, France

[2] Laboratoire Ondes et Acoustique, Ecole Supérieure de Physique et de Chimie Industrielles, 10 rue Vauquelin, 75005 Paris, France

E-mail: cuypers@pmmh.espci.fr

Received 12 February 2004
Published 19 August 2004
doi:10.1088/1468-5248/5/1/030

Abstract. In a recent letter (Cuypers Y *et al* 2003 *Phys. Rev. Lett.* **91** 194502), the authors presented experimental results on a structure resulting from a vortex burst. The temporal evolution of this structure results in the $k^{-5/3}$ Kolmogorov spectrum and some common features with the Lundgren theoretical vortex have been shown. The purpose of the present paper is to go further in the comparison with the Lundgren model by a parallel analysis of the experimental structure and of a Lundgren single spiral vortex, whose evolution is numerically obtained based on the calculations of Pullin *et al* (1993 *Phys. Fluids* A **5** 126; 1994 *Phys. Fluids* **6** 3010).

PACS numbers: 47.32.Cc, 47.27.Eq

JoT 5 (2004) 030

 PII: S1468-5248(04)76058-0 1468-5248/04/000001+22$30.00

Contents

1. Introduction

Numerous numerical simulations and experiments have shown the presence of coherent structures concentrating vorticity of turbulent flows [1, 2], introducing by the way, the idea that statistical laws in turbulence might be controlled by discrete structures. There have been several attempts to model turbulence using collections of coherent structures [3]–[6]; for an interesting review see [7]. To provide a satisfactory modelling of turbulence, these models must be able to reproduce the $k^{-5/3}$ law, predicted by Kolmogorov [8] and verified in many experiments. This was not achieved in [4]–[6]. The first model based on Burgers sheets and tube vortices proposed in 1951 by Townsend [4] leads to a k^{-1} spectrum for vorticity tubes, and to a k^{-2} spectrum for vorticity sheets. The $-5/3$ exponent of Kolmogorov lies between these two values, suggesting that a more complex structure having both a tube- and sheet-like character might be a good candidate. Such a structure was proposed by Lundgren in 1982 [3] in the form of an unsteady stretched spiral

vortex. Lundgren showed that a dynamical model of isotropic turbulence based on an ensemble of these structures at different ages of evolution, effectively reproduces the $k^{-5/3}$ spectrum. The Lundgren spiral vortex is an asymptotic solution of the Navier–Stokes equation, consisting of the superposition of a two-dimensional (2D) rotational flow and a uniform straining irrotational flow stretching the vorticity along the vortex axis. To perform the calculation of the spectrum over the N vortices, an ergodicity hypothesis is used: the energy spectrum $E(k)$ of N vortices is written as $E(k) = \sum_{n=1}^{N} E_n(k) = \mathcal{N} \int_{t_1}^{t_2} E(k,t)\,\mathrm{d}t$, where t_1 and t_2 are, respectively, the instants of creation and destruction of the structure, and $\mathcal{N}$ the rate of production and destruction of the vortices. Therefore, the $k^{-5/3}$ spectrum results from the time-averaged energy spectrum over a single structure lifetime. In this model, the energy cascade process leading to the $k^{-5/3}$ spectrum can be understood as the decrease with time of the space separating two successive turns of the spiral. This evolution results in the combination of the differential rotation imposed by the core which wind up the vorticity and the contraction due to the stretching. The Lundgren vortex is an asymptotic solution of the Navier–Stokes equation valid for long time where the initial spiral structure plays the role of a free parameter. The initial process leading to such a spiral vortex is therefore not contained in the model. However, several mechanisms such as vortex coalescence, roll-up of shear layers or wavy instabilities are known to produce spiral structures. The general idea is that nonuniformities in the vortex cross-sections resulting either from vortex instabilities or coalescence with neighbours are sheared and lumped into vorticity sheets by the differential rotation, and are idealized in the model as a spiral structure. This hypothesis was tested in [9], where Lundgren reformulated the model in such a way that the strictly 2D part of the flow can be separated from the straining part of the model. The 3D energy spectrum can therefore be calculated from the enstrophy spectrum of the 2D unstrained flow by a simple transformation. The main advantage of this reformulation is that the 2D enstrophy spectrum can be obtained numerically from any vortical flows, and not only from the asymptotic analytical solution.

Lundgren's mechanism for the build-up of the energy cascade has initiated a field of research whose results show nice predictions for turbulent flows [10, 11]. However, despite the fact that spiral structures have been identified in turbulent flows [12, 13], experimental evidence showing that these structures are responsible for the $k^{-5/3}$ part of the spectrum is still lacking. In a recent letter [14], the authors have presented experimental results on a structure resulting from a vortex burst and have shown that this structure shares some common features with Lundgren's theoretical one. The studied flow is a unique vortex whose environment causes it to break periodically into a turbulent burst. In contrast with classical experiments focusing on coherent structures in turbulence, no surrounding turbulent flow exists, so that the observed turbulence results only from the vortex burst. In agreement with Lundgren's theory, it has been found that the energy spectrum is time-dependent and does follow a five-thirds law when averaged over the lifetime of the vortex burst. In the present paper, interest is in comparing in more detail the temporal evolution of our experimental structure and a single spiral structure evolving according to Lundgren's mechanism. This is done through qualitative comparison of the vorticity fields and through quantitative comparisons of the time evolution of the energy spectra. The paper is embellished with several animations and visualizations to give a communicative representation of the computed quantities.

2. Experimental set-up

We describe in this section the experimental set-up in which the turbulent vortex burst periodically occurs. In addition to PIV measurements of the vorticity field, the main quantitative data are obtained using a hot-film probe. The recording data are rescaled benefiting from the

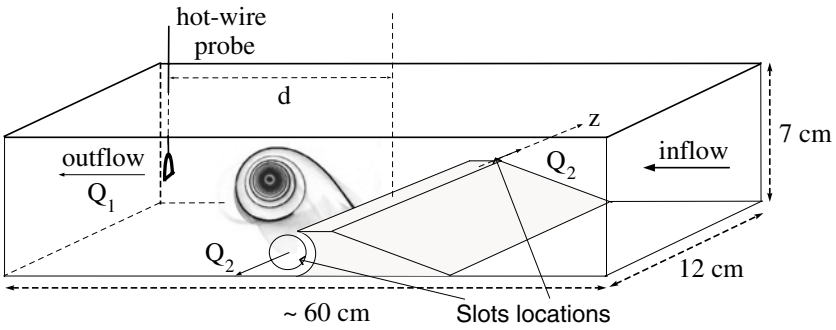

Figure 1. Working section of the hydrodynamic channel. The vorticity contained in the lower boundary layer is enhanced by the addition of a small step and stretched by a suction through two slots in the lateral wall to generate a strong stretched vortex; see also animation 1.

periodicity of the phenomenon and exploit via a local Taylor hypothesis to build the power spectrum density (velocity PSD) in the spectral k domain. Finally, we introduce the notion of instantaneous/cumulative PSD that will be used later in the paper to compare with the Lundgren vortex model.

2.1. Experimental set-up and vortex burst characteristics

The experiment is performed in a water channel, where the flow is generated by gravity from a constant level tank. The channel of $2m$ length is made of Plexiglas. It consists of two sections: the first section generates a laminar flow and the second is the working section. The working section is represented in figure 1. Its cross-section is $7\,\mathrm{cm} \times 12\,\mathrm{cm}$ and the typical longitudinal velocity is a few $\mathrm{cm\,s^{-1}}$. At the middle of the working section, a small step (5 mm height) added to the laminar boundary layer profile of the bottom wall produces the initial vorticity. This initial vorticity is strongly enhanced by the stretching produced by sucking the flow through slots on each lateral wall (slot diameter is 0.6 cm) which are aligned with the step axis. A stretched vortex is produced, whose axis is attached at both extremities to the suction slots. A video of the experimental set-up and of the vortex generated is given in animation 1. At fixed suction flowrate Q_2, varying the downstream flowrate Q_1 leads to the occurrence of two regimes, low values of Q_1 correspond to a stable, nearly stationary vortex. Above some critical value of Q_1 (not discussed here), the vortex follows a periodic cycle: in the first stage of the cycle, it remains coherent while it is elongated under the influence of the flow, and in the second stage, it explodes in a turbulent burst; thereafter another vortex is generated and so on. The two stages of the cycle are illustrated in figure 2 that shows two different visualizations:

- A cross-sectional visualization using a fluorescent dye sheet injection plus an illumination with a laser sheet.
- A top view visualization, using colorant dye injected through small inox tubes. An animation of this last visualization is given in animation 2.

Care has to be taken on the streak lines observed in figure 2(a) that takes the form of a spiral. This does not correspond to the vorticity field, axisymmetric at this stage (see [15]). It should also be noticed that the second stage of the flow, referred as the turbulent burst, still shows some coherence; this can be guessed from figures 2(c) and (e) and will be made clear from PIV measurements in section 4.1. The two stages have roughly the same duration $T \simeq 5\,\mathrm{s}$ and a whole cycle has a period $T_{cycle} \simeq 10\,\mathrm{s}$. In previous studies, the vortex has been characterized

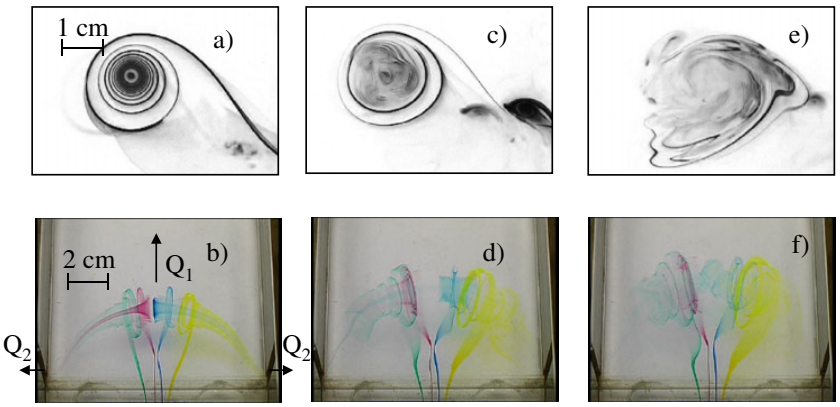

Figure 2. Sketch of the vortex cycle at $Q > Q_c$. First stage of the cycle, the vortex is still coherent; (a) side view and (b) top view. Second stage of the cycle; the vortex breaks into a turbulent burst; (c–e) side view and (d–f) top view. See also animation 2.

Table 1. Characteristics of the vortex when it breaks. u_θ^{max} denotes the maximum azimuthal velocity $u_\theta(r)$, reached for $r = r_0$ (r_0 the vortex core size), Γ denotes the circulation and R the lateral extension of the vorticity (the corresponding measurements can be found in [15]). Finally, a coarse estimation of the stretching $a \equiv \partial_z u_z$ is given (from [18]).

u_θ^{max}	r_0	Γ	$Re = \Gamma/\nu$	R	a
$10\,\mathrm{cm\,s^{-1}}$	0.6 cm	$40\,\mathrm{cm^2\,s^{-1}}$	4000	∼3 cm	$1\text{–}10\,\mathrm{s^{-1}}$

in terms of a coherent structure in both stable and unstable regimes [15]–[18]. Benefiting from previous measurements [15], we report in table 1 the characteristics of the vortex when it breaks (in the present experiments, $Q_1 = 12.5\,\mathrm{l\,min^{-1}}$ and $Q_2 = 7.5\,\mathrm{l\,min^{-1}}$). Since measurements of the axial velocity $u_z(z)$ is not possible in the periodic regime, only a coarse estimation of the stretching $a \equiv \partial_z u_z$ is given, corresponding to measurements performed in the stable regime [18].

2.2. PIV and hot-film measurements

To characterize the experimental vortex structure, we performed PIV measurements in a cross-section of the vortex at the middle of the channel ($(r, \theta, z = 0)$ plane). Our PIV system comprises a high-resolution camera (1280×1024 pixels) capturing images at a frequency of 4 Hz and a double-pulsed Nd:YAG delivering 12 mJ at each pulse. The experimental apparatus is sketched in figure 3. The measurement area, $9\,\mathrm{cm} \times 7\,\mathrm{cm}$, is large enough to give a picture of the whole turbulent burst whose lateral extension is $R \simeq 3\,\mathrm{cm}$. The interrogation cell is 16×16 pixels with a 50% overlap, leading to a spatial resolution of 128×160 vectors. The resulting space tick between two vectors is $\delta l = 0.5\,\mathrm{mm}$. The PIV works as a low-pass filter since it cannot resolve scales smaller than δl. Since the dissipative scale in our experiments is k_M with $10 \leq k_M \leq 34\,\mathrm{cm^{-1}}$ (see section 4.2), the resolution is sufficient to capture the scales in the inertial range. At this stage we have not performed a quantitative analysis of the PIV measurements. Indeed, computations of quantities like the energy spectrum can only be obtained

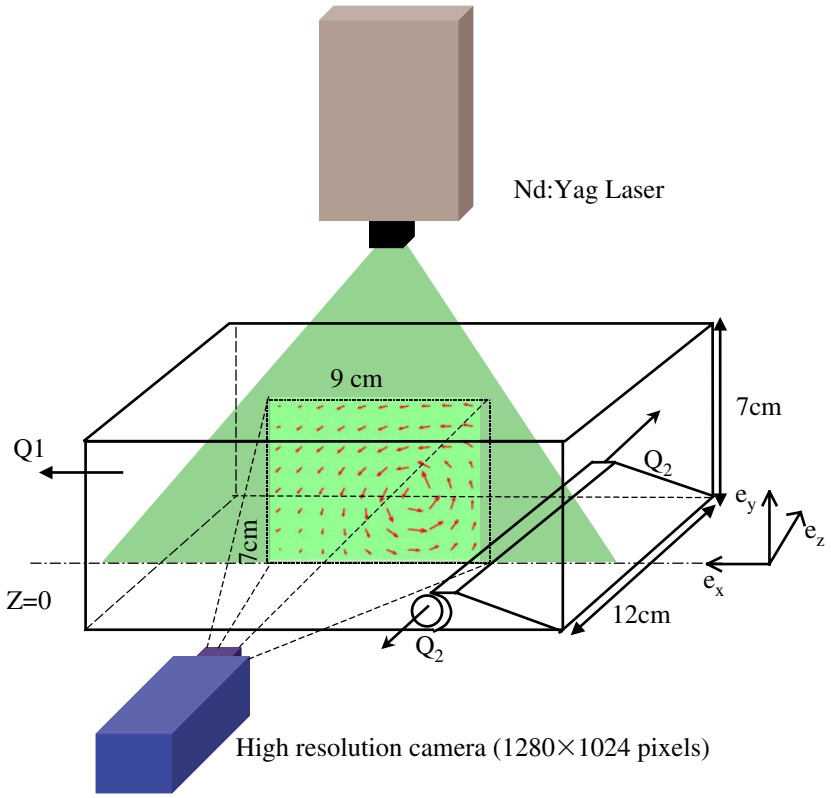

Figure 3. Experimental set-up for PIV measurements.

via an ensemble averaging over N PIV velocity fields, where N is large enough to obtain statistical convergence of the computed quantities. Since the energy spectra are time-dependent, such an averaging is only valid if the acquisition of the PIV images is synchronized with the burst period. Work is in progress in that direction. Therefore, we give only a qualitative analysis of the PIV measurements via visualizations of the instantaneous vorticity field of the burst in section 4.1.

To quantify the burst, local measurements of the velocity have been taken using a hot-film probe, located at a distance d from the z-axis, as indicated in figure 1. The probe is set parallel to the axis of the stretching so that it measures $U = \sqrt{u_r^2 + u_\theta^2}$. A typical time recording is shown in figure 4. It is composed of several periodic cycles, each cycle being formed of two parts: in the first one, the velocity increases smoothly, whereas the second one shows strong fluctuations with a global decrease in the velocity. A visualization during one cycle has been performed using fluorescein illuminated with a laser sheet in the plane $(r, \theta, z = 0)$. This visualization (the probe location is shown by a red cross) and the corresponding velocity signal U are reproduced in animation 3. In the first part of the animation, the vortex, still coherent, is advected from the left under the effect of the downstream flow. The corresponding recorded velocity smoothly increases because the vortex brings a stronger and stronger velocity contribution as it comes closer and closer to the probe. The second part of the animation shows the vortex burst, followed by a growing turbulent mixing region of the fluorescent dye inside the laminar flow. In the velocity signal, it corresponds to strong fluctuations superimposed to a mean velocity. Finally, the animation shows the relaminarization of the flow, whereas another vortex appears from the left, advected by the downstream flow, that will experience a similar scenario.

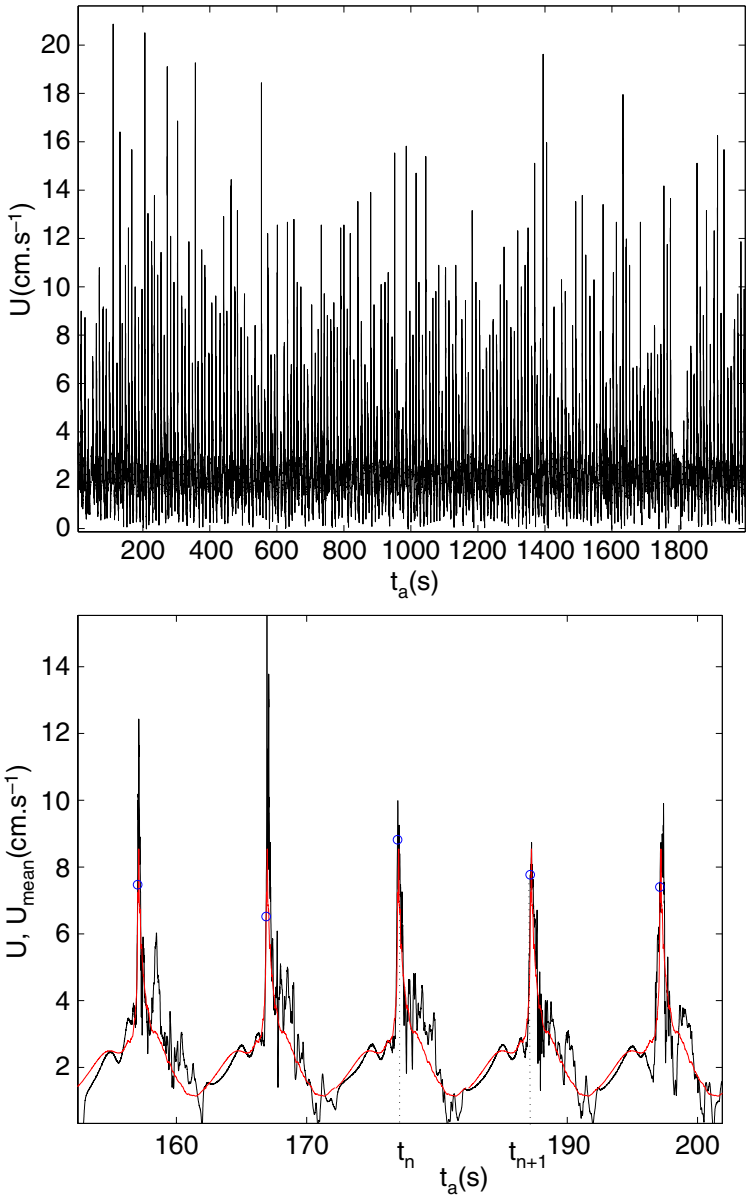

Figure 4. (a) Full temporal recording of the velocity $U(t_a)$ (t_a denotes the absolute time). (b) Close up of the temporal recording over several vortex cycles $U(t_a)$; the mean velocity U_{mean} is indicated by red line and ○ indicates the times t_n at which the vortex breaks on each cycle; see also animation 3.

2.3. Data processing

2.3.1. Defining the mean velocity. Time recording data $U(t_a)$ (where t_a denotes absolute time) is periodic with a mean periodicity T_{cycle}. This allows to define a mean velocity U_{mean} over a cycle via a coherent cycle averaging technique (note that, physically, U_{mean} results from both the remaining downstream flow and from the rotation induced by the vortex core). We compute the intercorrelation function of the whole signal U with $U_m^{(0)} = U(t^{(0)} \rightarrow t^{(0)} + T_{cycle})$, a part of the signal U starting at some arbitrary time $t^{(0)}$ in the laminar region, and whose length is T_{cycle}

(we denote by $U(t \to t')$ the part of the signal U truncated from t to t'). The maxima of the intercorrelation function give the approximative times $\{t_n^{(1)}\}_{n=1,\ldots,N}$ for the beginning of the N cycles, and the ensemble average $U_m^{(1)} = (1/N)\sum_{n=1}^{N} U(t_n^{(1)} \to t_n^{(1)} + T_{cycle})$ a first evaluation of the mean velocity. In the next step, the intercorrelation of the signal U using $U_m^{(1)}$ (instead of $U_m^{(0)}$) gives a new set of initial times $\{t_n^{(2)}\}_{n=1,\ldots,N}$ and a new mean velocity $U_m^{(2)}$. The operation is iterated j times until $U_m^{(j)}$ has converged with a desired accuracy, and we denote by U_{mean} the converged mean velocity (and $\{t_n\}_{n=1,\ldots,N}$ the corresponding times). Different choices for $t^{(0)}$ will mainly result in shifted values of $\{t_n\}$ and in a corresponding shifting of U_{mean}, this shifting will not affect further calculations.

2.3.2. Defining initial and final times of the turbulent burst. Heuristically speaking, we define the initial time of a cycle as the beginning of the second stage on each cycle!

Actually, we give in our study a very particular sense to the initial time: it is the time where the turbulent spectrum (with $k^{-5/3}$ range) starts to build up. Since we need to use the averaged spectra $e_{\Delta t}(k,t)$ to define this time (see section 2.4), the discussion on the determination of this initial time is given in the appendix.

Final time has a less important definition. It could be defined as the initial time plus T_{cycle}; in that case, the first stage where the flow is laminar would be included. We prefer to focus on the second stage and, thus, the final time is here defined as the initial time plus T (the duration of the second stage). It is shown in the appendix that this definition is satisfactory in the sense that T is larger than the duration of the turbulent cascade build-up.

In the following, the set of initial times $\{t_n\}_{n=1,\ldots,N}$ is chosen to be equal to the initial times of the turbulent burst.

2.3.3. Defining the fluctuating velocity on each cycle. The U_{mean} and the corresponding $\{t_n\}_{n=1,\ldots,N}$ being obtained as described above, data are rescaled as follows:

$$u_n(t) = U(t_a = t_n \to t_n + T) - U_{mean}(t), \tag{1}$$

where $t = 0 \to T$ is a new time. The N signals $u_n(t)$ correspond to the velocity fluctuations in the second stage of each cycle, i.e. from the initial time t_n to the final time, T (figure 4(b)).

2.3.4. The local Taylor hypothesis. The hot-film measurement provides a one-point time recording of the velocity. Since theoretical predictions are usually made in the spatial domain or spectral k domain, we need to obtain spatial scales from time scales. This is achieved using the local Taylor hypothesis $r = \int_0^t U_{mean}(t')\,\mathrm{d}t'$ (this definition will be slightly adapted in section 2.4). This hypothesis, firstly advocated in [19] and which can also be found detailed in [20]–[22], reduces the bias the classical Taylor hypothesis (of frozen turbulence) introduces on the velocity signal when large velocity fluctuations are considered (in our case $\langle (U - \langle U_{mean}\rangle)^2\rangle / \langle U_{mean}\rangle$ is of order 30%, where $\langle\,\rangle$ indicates a time average). Using a local Taylor hypothesis, we take into account the advection of small scales by large scales that can be pictured here by the advection of the fine-scale structures of the turbulent spot by the vortex-core-induced motion (see figure 5).

We now work with the N signals $u_n(r)$:

$$u_n\left(r = \int_0^t U_{mean}(t')\,\mathrm{d}t'\right) = u_n(t). \tag{2}$$

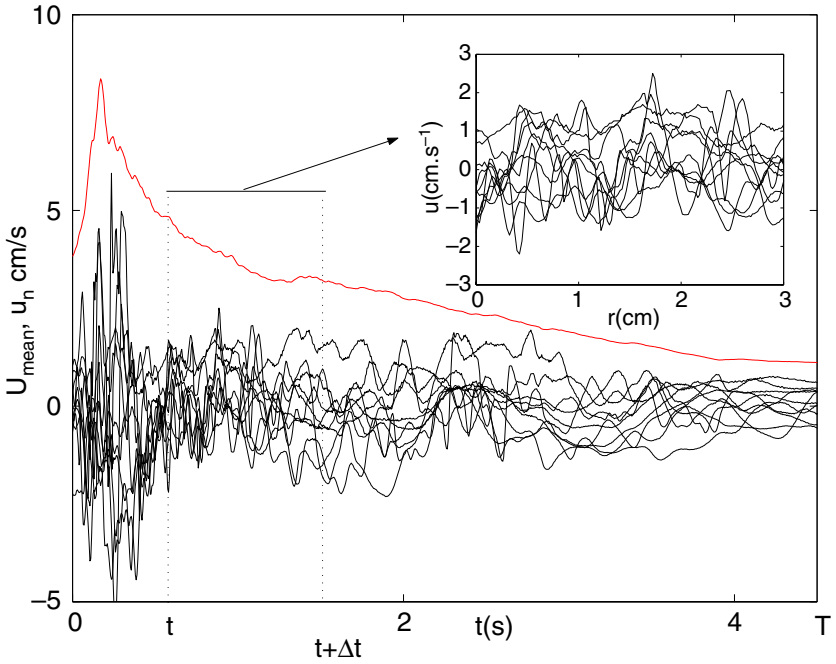

Figure 5. Result of the transformation $\delta t \to \delta r(t) = U_{mean}(t)\delta t$ using the local Taylor hypothesis on a temporal window $[t; t + \Delta t]$.

2.4. Cumulative/instantaneous velocity PSD

2.4.1. The averaged velocity PSD. The usual velocity PSDs are built as follows:

$$E(k) = \frac{1}{N}\sum_{n=1}^{N} E_n(k), \tag{3}$$

where $E_n(k)$ is the velocity PSD of $u_n(r)$, defined in (2) for $r = 0$ to $\int_0^T U_{mean}(t')\,\mathrm{d}t'$.

In this definition, the spectrum $E(k)$ results both from a time integration over the duration T of the burst and from an ensemble average over the N signals. The convergence of the spectrum in terms of ensemble average is obtained with 1% accuracy for 100 cycles averaging. In the following, the spectra are obtained with typically 200 cycles ensemble averaging. It is this spectrum that is expected to show an inertial range $[k_m; k_M]$ with $k^{-5/3}$ behaviour (see section 4.2).

2.4.2. The instantaneous velocity PSD. We define the instantaneous velocity PSD $e(k, t)$ as the ensemble average (average over the N signals) of the k spectra taken at a given time t in the turbulent burst (thus, $E(k) = \int_0^T e(k, t)\,\mathrm{d}t$). The natural way to obtain these spectra would be to take the Fourier transform of the velocity field in the physical space $u(\boldsymbol{x}, t)$ (for instance, from PIV images). As previously said, this is not possible and we choose an alternative procedure.

Let us consider a slightly modified formulation of the local Taylor hypothesis (2):

$$u_n(r = 0 \to \Delta r) = u_n(t \to t + \Delta t), \tag{4}$$

where

$$r = \int_t^{t+\delta t} U_{mean}(t')\,\mathrm{d}t', \tag{5}$$

with

$$r \leq \Delta r = \int_{t}^{t+\Delta t} U_{mean}(t')\,\mathrm{d}t' \quad \text{for } \delta t \leq \Delta t. \tag{6}$$

Working with this temporal window $[t; t+\Delta t]$ allows one to solve, in the k domain, the scales between 0 and Δr that are detected by the probe during that time. The corresponding spectrum is defined by

$$e_{\Delta t}(k,t) = \frac{1}{N}\sum_{n=1}^{N} e_{n,\Delta t}(k,t), \tag{7}$$

where $e_{n,\Delta t}(k,t)$ is the velocity PSD of $u_n(r)$, defined in (4) for $r=0$ to Δr. The physical meaning of $e_{\Delta t}(k,t)$ is an average of the spectra between t and $t+\Delta t$. When Δt tends to zero, $e_{\Delta t}(k,t)$ tends to the instantaneous spectrum $e(k,t)$. However, since in that procedure, a small Δt implies a small Δr (and thus a less resolved spectrum), a balance has to be chosen between the precision on time t and the quality required for the spectrum calculation.

We are interested in studying the behaviour of the instantaneous spectra in the inertial range $[k_m; k_M]$ (fixed by the behaviour of $E(k)$). When decreasing Δr, the first resolved k value (except $k=0$) is given by $1/\Delta r$ and can thus overtake k_m. To give a consistent representation of the spectra, we use the following criterion: Δr (and thus Δt) is chosen in such a way that at least 80% of the inertial range is kept.

Finally, if Δt becomes of order T, i.e. Δt cannot be considered as small, the significance of $e_{\Delta t}(k,t)$ is rather an averaged spectrum over the duration Δt, starting at t (as in figure 8).

2.5. The cumulative velocity PSD

The cumulative velocity PSD is simply defined as $E^c(k,t) = \int_0^t e(k,t')\,\mathrm{d}t'$. With our experimental procedure, this means $E^c(k,t) \simeq e_{\Delta t=t}(k,0)$. This spectrum is the mean value of the instantaneous spectra between the initial time $t=0$ of the turbulent burst and time t between 0 and T. Consequently, we have, by definition $E(k) = E^c(k,T)$.

The cumulative spectrum allows one to accurately define the time T_v of the cascade build-up (see section 5.1).

3. Numerical calculation of Lundgren's single spiral model

We give in this section the main characteristics of the Lundgren vortex mechanism. This mechanism is simple and the model is flexible since the initial condition appears as a free parameter, allowing for applications to many flow configurations. Probably, the Lundgren vortex mechanism captures the essence of the turbulent process in the physical space: if in some place of the flow, a local stretching exists, any nonaxisymmetric vorticty in the, locally, perpendicular plane will be rolled-up (this is a bidimensional mechanism), whereas the stretching produces a radial compression of the rolled-up structure. It is this latter compression, combined with differential rotation, that is responsible for the transfer from large to small scales in the physical space since the radial distance between turns decreases.

We have chosen an initial condition for the numerical calculations borrowed from Pullin and Saffman [10, 23] in the form of a single spiral. Although this condition appears to differ from our experimental initial condition, it allows a comparison in the generic process of turbulent cascade build-up, which is done in sections 4 and 5.

3.1. The characteristics of the Lundgren model

In the Lundgren model [3], a solution of Navier–Stokes equations is sought of the form $(u_r, u_\theta, u_z) = (-ar/2 + v_r(r,\theta,t), v_\theta(r,\theta,t), az)$. Such a solution corresponds to a time-dependent z-vorticity $\omega^{3D}(r,\theta,t) = (\partial_r(rv_\theta) - \partial_\theta v_r)/r$ submitted to a stretching $\partial_z u_z = a$ along the z-axis. The total velocity field is three-dimensional but it can be shown that the equations reduce to a bidimensional dynamics for the vorticity $\omega(\rho,\theta,\tau)$ defined by

$$\omega^{3D}(r,\theta,t) = \mathrm{e}^{at}\omega(\rho,\theta,\tau), \tag{8}$$

with $\rho = r\mathrm{e}^{at/2}$ and $\tau = (\mathrm{e}^{at}-1)/a$ (ω is found to be solution of the bidimensional equation for the vorticity). An asymptotic solution (for long time) for ω is found by Lundgren in the form

$$\omega(\rho,\theta,\tau) = \sum_{-\infty}^{\infty} \hat{\omega}_n(\rho,\tau)\mathrm{e}^{\mathrm{i}n\theta}, \tag{9}$$

$$\hat{\omega}_n(\rho,\tau) = f_n(\rho)\mathrm{e}^{-\mathrm{i}n\Omega(\rho)\tau - \nu n^2\Lambda^2(\rho)\tau^3/3}, \tag{10}$$

where

$$\frac{1}{\rho}d_\rho(\rho^2\Omega(\rho)) = f_0(\rho) \quad \text{and} \quad \Lambda = d_\rho\Omega(\rho) \tag{11}$$

and $f_n(\rho)$ are arbitrary functions. The circulation of the whole structure is given by

$$\Gamma(r,t) = 2\pi\int_0^r f_0(\rho')\rho'\,\mathrm{d}\rho'. \tag{12}$$

To get insights of the form of this solution, let us recall the inviscid case with particular initial condition $f_n(\rho) = f(\rho)$ for $n \neq 0$. Using $\iint \delta(\theta - \Omega\tau)\mathrm{e}^{-\mathrm{i}n\theta}\mathrm{d}\theta\mathrm{e}^{-\mathrm{i}n\Omega\tau}$, one gets

$$\omega^{3D}(r,\theta,t) = \mathrm{e}^{at}\{f_0(\rho) + f(\rho)\delta(\theta - \Omega(\rho)\tau)\}. \tag{13}$$

This corresponds to a spiral of vorticity evolving through $(\theta, r = \mathrm{e}^{-at/2}\Omega^{-1}(\theta/\tau))$, with $\Omega(\rho)$ being dependent on the axisymmetric rotation $f_0(\rho)$.

Adding the effect of viscosity in (13) allows for accounting for the vorticity diffusion of the spiral and gives

$$\omega^{3D}(r,\theta,t) = \mathrm{e}^{at}\left\{f_0(\rho) + 2f(\rho)\sum_{n=1}^{\infty}\cos(n(\theta - \Omega(\rho)\tau))\mathrm{e}^{-\nu n^2\Lambda^2(\rho)\tau^3/3}\right\}. \tag{14}$$

3.2. Calculation of the vorticity field

In the following discussion, R denotes the lateral extension of the vortex at $t = 0$, Γ_0 the typical circulation, $\delta = \sqrt{\nu/a}$ the Burgers vortex radius and we use the nondimensional parameters $Re = \Gamma_0/\nu$ and $\alpha = \delta^2/R^2$; also, nondimensional time $T = a\tau$ and $\xi = \rho/R$ are used. Following [10, 23], we define the functions f_0 and f as

$$f_0(\rho) = \alpha Rea\tilde{f}(\xi) = \alpha Re\frac{a}{\pi}\left(\frac{1}{C\sqrt{\xi}} - \xi^2\right)\mathrm{e}^{-\xi^2}, \tag{15}$$

$$f(\rho) = \alpha Rea f(\xi) = -\alpha Re \frac{a}{\pi} \xi^2 \mathrm{e}^{-\xi^2}, \tag{16}$$

where $C = \gamma(0.75)$ (with γ being the gamma function). The choice of these functions ensures $\Gamma(\infty, t) = 0$ and $\Omega(\rho)$ decreasing (or $\Lambda(\rho) < 0$). We use also, in the following,

$$\Omega(\rho) = \alpha Rea\, \tilde{\Omega}(\xi), \qquad \text{thus} \qquad \frac{1}{\xi} d_\xi(\xi^2 \tilde{\Omega}(\xi)) = \tilde{f}_0(\xi), \tag{17}$$

$$\Lambda(\rho) = \alpha Re \frac{a}{R} \tilde{\Lambda}(\xi), \qquad \text{thus} \qquad \tilde{\Lambda}(\xi) = d_\xi \tilde{\Omega}(\xi). \tag{18}$$

Solution (13) is written as

$$\omega^{3D}(r, \theta, t) = \mathrm{e}^{at} \alpha Rea\, \tilde{\omega}(\xi, T), \tag{19}$$

$$\tilde{\omega}(\xi, T) = \tilde{f}_0(\xi) + 2\tilde{f}(\xi) \sum_{n=1}^{\infty} \cos(n(\theta - \alpha Re \tilde{\Omega}(\xi) T)) \mathrm{e}^{-n^2 \alpha^3 Re^2 \tilde{\Lambda}^2(\xi) T^3/3}. \tag{20}$$

For given Re and α, it is easy to compute $\tilde{\omega}^N(\xi, T)$ in (20) where the series are truncated at N terms such that $|\tilde{\omega}^N(\xi, T) - \tilde{\omega}^{N-1}(\xi, T)| < \epsilon\, |\tilde{\omega}^N(\xi, T)|$ with ϵ being the desired accuracy. In our calculation, ϵ is set equal to 10^{-4}.

3.3. Calculation of the energy spectrum

In [3, 10, 23] the total energy spectrum is written as $E_0(k) + E(k)$, where $E_0(k)$ refers to the axisymmetric contribution and

$$E(k) = \int_{\tau_1}^{\tau_2} e(k, \tau)\, \mathrm{d}\tau, \tag{21}$$

$$e(k, \tau) = \frac{2\pi \mathcal{N}}{k} \sum_{n=1}^{\infty} |I_n(k, \tau)|^2, \tag{22}$$

$$I_n(k, \tau) = \int_0^{\infty} J_n\left(\frac{k\rho}{\sqrt{1 + a\tau}}\right) \hat{\omega}_n(\rho, \tau) \rho\, \mathrm{d}\rho, \tag{23}$$

where $\mathcal{N}$ denotes a production of vortex length per unit time (in the following, $\mathcal{N} R^2/a$ is set to 1).

The time integral $E(k)$ is shown to be split into a contribution of order O(1) for $a\tau < 1$ and a contribution of order O($a\tau$) for $a\tau > 1$ [10]. This latter contribution is responsible for the range in $k^{-5/3}$. Thus, neglecting terms of O(1) gives the famous Kolmogorov law!

A detailed discussion on the early and late cutoff times τ_1 and τ_2 and their physical meaning can be found in [10, 23]. In our computation, we retain the value $\tau_1 = \phi/a$ with $\phi = 0.475$, chosen in [10], and we checked that the time integral for $E_s(k)$ has converged for $\tau_2 = C/(4aRe^{2/3}\alpha)$ where $C \simeq 10$ in [10].

We introduce the nondimensional wavenumber $K = kR$ and the functions

$$E(k) = 2\pi\alpha^2 Re^2 R^3 a^2\, \tilde{E}(K), \tag{24}$$

$$e(k,\tau) = 2\pi\alpha^2 Re^2 R^3 a^3\, \tilde{e}(K,T), \tag{25}$$

$$I_n(k,\tau) = \alpha Re R^2 a\, \tilde{I}_n(K,T). \tag{26}$$

To compute $e_s(k,\tau)$ and $E_s(k)$, we use the same approximation as in [3, 10]. For $K > 1$, the asymptotic form of the Bessel function $J_n(z) \simeq \sqrt{2\pi/z}\,\cos(z - n\pi/2 - \pi/4)$ is written as

$$\tilde{I}_n(K,T) = \sqrt{2\pi}\int_0^\infty A_n(\xi)(\mathrm{e}^{\mathrm{i}\varphi_n(\xi)} + \mathrm{e}^{\mathrm{i}\varphi_n^v(\xi)})\,\mathrm{d}\xi \tag{27}$$

$$= \pi\frac{A_n(\xi_n)}{\sqrt{\varphi''(\xi_n)}}\exp(\mathrm{i}(\phi_n(\xi_n) + \pi/4)), \tag{28}$$

where

$$A_n(\xi) = \left(\frac{\sqrt{1+T}}{K}\right)^{1/2} \xi\tilde{f}(\xi)\mathrm{e}^{-n^2\alpha^3 Re^3\tilde{\Lambda}^2(\xi)T^3/3}, \tag{29}$$

$$\varphi_n(\xi) = -n\alpha Re\tilde{\Omega}(\xi)T - \frac{K\xi}{\sqrt{1+T}} + \frac{\pi}{4}(2n+1). \tag{30}$$

Here, we have used the stationary-phase evaluation, with ξ_n given by the implicit relation $(\varphi'(\xi_n) = 0)$

$$n\alpha Re\tilde{\Lambda}(\xi_n)T\sqrt{1+T} + K = 0. \tag{31}$$

As it has been assumed that $\tilde{\Lambda}(\xi) < 0$, the integral of the term with phase $\varphi_n^v(\xi) = -n\alpha Re\tilde{\Omega}(\xi)T + (K\xi/(\sqrt{1+T})) - (\pi/4)(2n+1)$ vanishes. We can now write

$$\tilde{e}(K,T) = \frac{1}{K}\sum_{\xi_{n=1}}^{\infty}\frac{|A_n(\xi_n)|^2}{|\varphi''(\xi_n)|} \tag{32}$$

$$= -\frac{1+T}{K^3}\exp\left(-\frac{2\alpha T K^2}{3(1+T)}\right)\sum_{\xi_{n=1}}^{\infty}\xi_n|\tilde{f}(\xi_n)|^2\frac{\tilde{\Lambda}(\xi_n)}{\tilde{\Lambda}'(\xi_n)}, \tag{33}$$

$$\tilde{E}(K) = \int_{T_1}^{T_2}\tilde{e}(K,T)\,\mathrm{d}T. \tag{34}$$

As shown previously, $\tilde{e}(K,T)$ can be evaluated by $\tilde{e}^N(K,T)$ truncating the series to the first N terms such that $|\tilde{e}^N(K,T) - \tilde{e}^{N-1}(K,T)| < \epsilon|\tilde{e}^N(K,T)|$. In our calculation, ϵ is equal to 10^{-4}. To evaluate $\tilde{E}(K)$, the following definition is introduced:

$$\tilde{E}^c(K,T) = \int_{T_1}^{T}\tilde{e}(K,T')\,\mathrm{d}T'. \tag{35}$$

This spectrum corresponds to the cumulative spectrum between T_1 and T and will be used in the comparison with experiments. Then, we numerically integrate (using a explicit Runge–Kutta scheme), for each value of K,

$$\frac{\partial\tilde{E}^c(K,T)}{\partial t} = \tilde{e}(K,T), \qquad \text{with initial condition} \qquad \tilde{E}^c(K,T_1) = 0. \tag{36}$$

It has been checked that $E^c(K,T)$ has converged with an accuracy of around 2% for each K when T reaches T_2 (thus $\tilde{E}(K) = \tilde{E}^c(K, T \geq T_2)$).

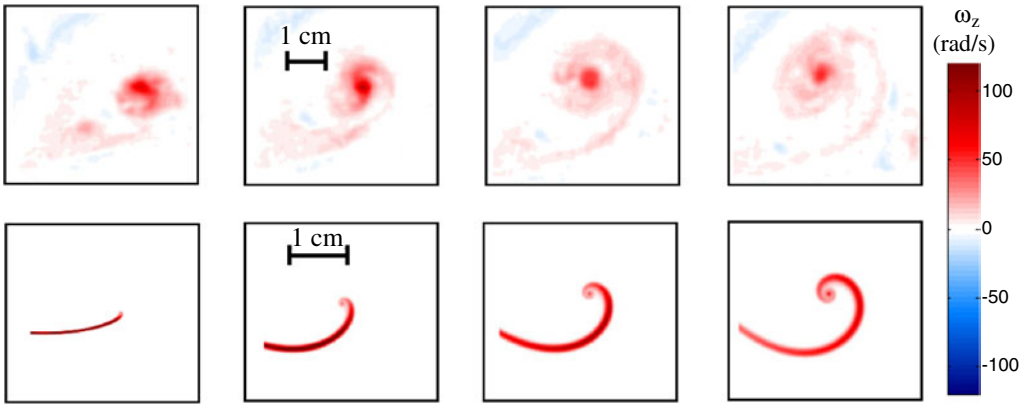

Figure 6. Visualization of the vorticity field ω_z. Top: experimental vorticity field; bottom: numerical PIV vorticity field. From left to right ($t - t_1 = 0.25$ s, $t = 0.5$ s, $t = 0.75$ s, $t = 1$ s); see also animation 4.

3.4. Nondimensional parameters in our calculations

In the discussion below, results have been obtained using the nondimensional parameters $Re = 4000$, $\alpha = 1/1395$, and time and space have been rescaled using $R = 3$ cm and $a = 1.55\,\mathrm{s}^{-1}$. The values chosen here corresponds to the experimental values of table 1. We choose the specific value $a = 1.55\,\mathrm{s}^{-1}$ in the experimental range $1\,\mathrm{s}^{-1} \leq a \leq 10\,\mathrm{s}^{-1}$ so that the numerical lifetime $t_2 - t_1$ exactly equals the experimental lifetime $T_v = 1.5$ s for the build-up of the cascade (which will be defined in section 5.1). Otherwise using the complete experimental range for a, leads to $0.5\,\mathrm{s} \leq t_2 \leq 2.5\,\mathrm{s}$.

4. A first qualitative comparison

We give in this section two qualitative comparisons between our experimental vortex and the Lundgren single spiral vortex. First the comparison is given with vorticity visualizations: if this kind of comparison could appear as the simplest way to quantitatively compare both vortexes, experimental limitations of PIV images have not allowed further analysis. However, it gives hints that our experimental vortex indeed experiences the kind of mechanism contained in Lundgren's model.

The second comparison is with the time-averaged velocity PSD $E(k)$. In both cases, the spectra are shown to have an inertial part with $k^{-5/3}$ behaviour whose range and time of build-up compare nicely.

4.1. Visualizations in the physical space

Animation 4 and figure 6 give the comparative temporal evolution of the vorticity $\omega_z = (1/r)((\partial/\partial r)rV_\theta - (\partial/\partial\theta)V_r)$ experimentally obtained from the PIV measurements and of the vorticity $\omega^{3D}(r, \theta, t)$ numerically calculated as described in section 3.2 (all quantities are in dimensional form). The initial time roughly corresponds to the beginning of the explosion in the experiment and to t_1 in the numerical calculation. The final time is $T_v = 1.5$ s, which is the experimental lifetime of our vortex. The time separating two successive images is 0.25 s.

The observed process in the experiments and in numerical calculations nicely compare in images 3 to 6 (animation 4). In both cases, the vorticity is concentrated in a spiral structure that evolves in time rolling up around the stretching axis.

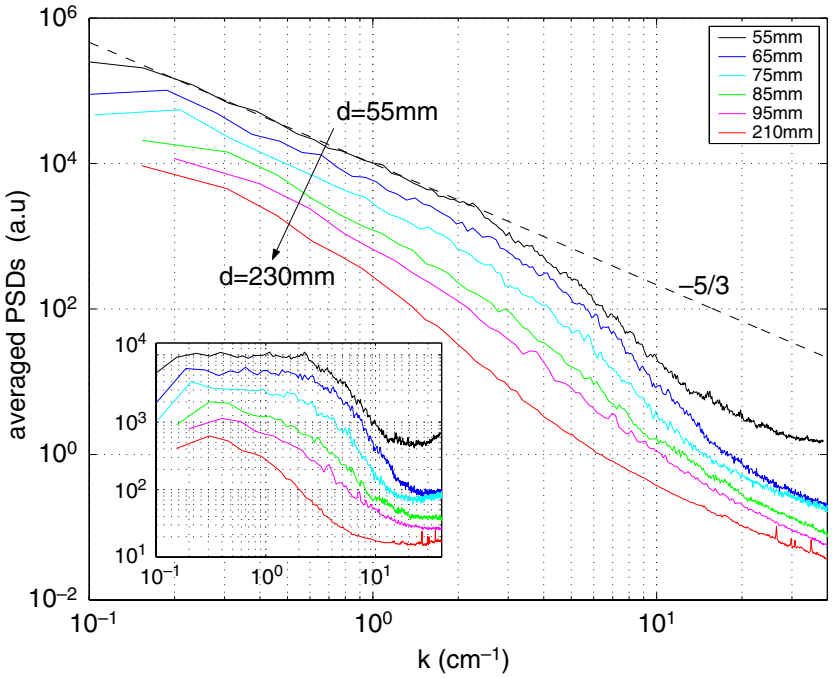

Figure 7. Experimental velocity PSDs averaged over the whole cycle $E(k) = e_T(k, 0)$ for various distances d of the probe from the z-axis ($d = 55$, 65, 75, 85, 95, 135 and 230 mm). The inset shows the compensated spectra $k^{5/3}E(k)$.

The process differs both at the beginning and at the end of the animation. The first images correspond to the initial condition. It is thus not surprising to observe a difference at this stage: our experimental initial condition is not single spiral arm, but rather a distribution of vorticity patches. In the last images, the turbulent cascade probably has yet to build up. In the numerical calculations, the structure tends to axisymmetry under the effect of the radial compression. In our experiments, this does not occur. The radial compression seems to vanish. This can be attributed to the following mechanism: when the vortex breaks, it can be seen from animation 2(b) that the structure is no more attached to the suction hole. One can guess that the stretching persists during some time, sufficient to allow the turbulent cascade (in the sense sought in the Lundgren mechanism) to process and, finally, vanishes after few seconds.

4.2. A turbulent spectrum in both cases!

We first report results on the experimental spectrum. Figure 7 shows the velocity PSDs averaged over the whole burst lifetime $E(k)$ as a function of the distance d from the z-axis. A clear $k^{-5/3}$ decay region of the energy spectrum is obtained in the region where the vortex explodes (here $d = 55$ mm). This result shows that the evolution of such a stretched vortex burst contains already all the dynamics for the generation of a Kolmogorov spectrum. The inertial range is $k_m \simeq 0.2\,\mathrm{cm}^{-1} \ll k \ll k_M \simeq 2\,\mathrm{cm}^{-1}$.

Figure 8 shows the spectra $e_{\Delta t \simeq T/3}(k, t)$ calculated for $d = 55$ mm and at $t = 0, T/3$, and $2T/3$, i.e. the three spectra averaged over each third of the burst life. Both figure 7 and 8 suggest that the turbulent vortex, i.e. leading to an inertial range with $k^{-5/3}$ behaviour, has a lifetime shorter than the burst duration T: the whole turbulent spectrum is built in a time T_v of around $T/3 \simeq 1.5$ s in the region where the vortex breaks (the value of T_v will be defined

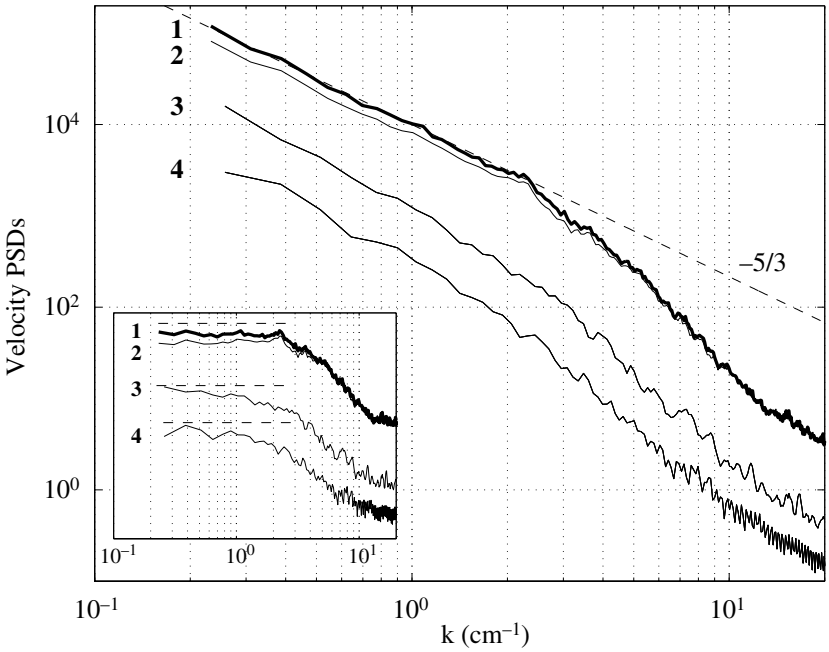

Figure 8. Experimental velocity PSDs averaged over a third cycle compared with the velocity PSD averaged over the whole cycle for $d = 55$ mm. Curve **1** denotes $E(k)$ averaged over the whole cycle, **2** denotes $e_{\Delta t=1.5\,\mathrm{s}}(k, t = 0)$ averaged over the first third cycle, **3** $e_{\Delta t=1.5\,\mathrm{s}}(k, t = 1.5\,\mathrm{s})$ averaged over the second third cycle and **4** $e_{\Delta t=1.5\,\mathrm{s}}(k, t = 3\,\mathrm{s})$ averaged over the last third cycle. The inset shows the corresponding compensated spectra $k^{5/3}e_{\Delta t}(k, t)$.

more precisely from figure 10). Thereafter, the turbulence decays (in time and space). It has to be noticed that the turbulence decay with time observed in figure 8 cannot be ascribable to a simple advection of the spot beyond the probe position. In that case, the whole turbulent spectrum would be recovered for further positions of the probe contrary to the results shown in figure 7.

In the Lundgren model, the averaged velocity PSD presents a $k^{-5/3}$ behaviour in an inertial range $[k_m; k_M]$, with $k_m = 1/R$ and $k_M = \sqrt{a/\nu}$. With the experimental values of table 1, one gets $k_m \simeq 0.3\,\mathrm{cm}^{-1}$ and $10\,\mathrm{cm}^{-1} \leq k_M \leq 34\,\mathrm{cm}^{-1}$ that reasonably compare with experimental inertial range.

Velocity PSD is numerically calculated as described in section 3.3, and the result is shown in figure 9. It can be seen that the numerical velocity PSD has a reduced inertial range. This is also observed in [10, 23] and can be attributed to the approximation used in the numerical calculations.

5. Evolution of the spectra: Lundgren's process versus experiments

To better understand the build-up of the $k^{-5/3}$ spectrum, we compare the temporal evolution of the spectra during $[0, T_v]$ in the experiments and in the numerical calculations of a single spiral vortex.

Several works concerning the Lundgren model show that, instantaneously, spiral structures give an energy spectra with k^p behaviour, where p is dependent on the considered structure

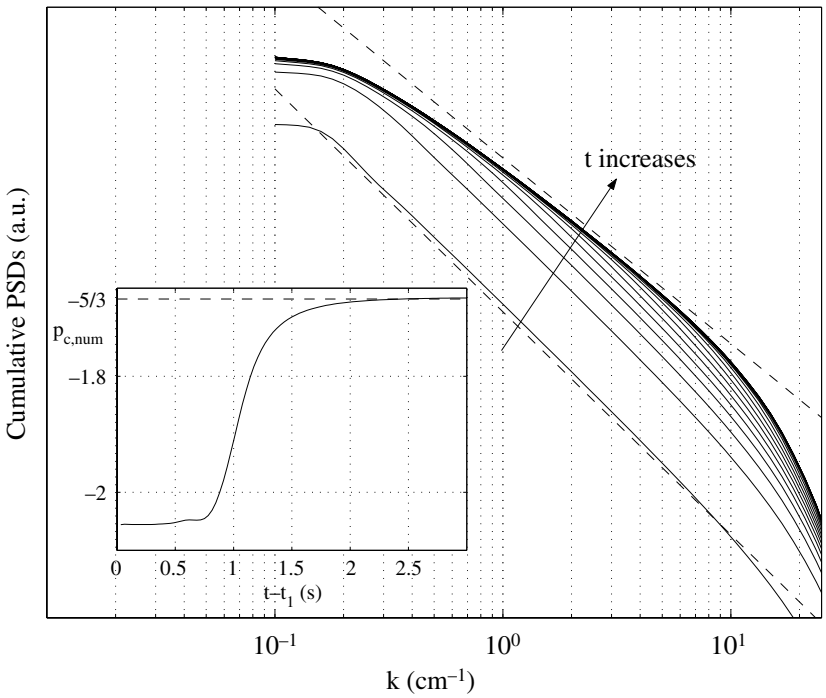

Figure 9. Numerical cumulative spectra $E^c(k,t)$ for increasing t (time spacing is equal to 0.16 s) for $a = 1.55\,\mathrm{s}^{-1}$, $\alpha = 1395$ and $Re = 4000$. Spectra have been calculated from $t_1 \simeq 0.25$ to 3 s, with $t_2 \simeq 1.75$ s. The inset shows the cumulative slope $p_{c,num}$ as a function of time (the origin corresponds to t_1).

[10, 24, 25]. For instance, Gilbert [24], applying Lundgren's ideas to a two-dimensional turbulent flow, showed that spiral structures have an energy spectra with $A(t)k^p$ behaviour for $k_1(t) < k < k_2(t)$. If the behaviours of $A(t), k_1(t), k_2(t)$ depend on the details of the spiral structure, one remarkable feature is that averaging over the lifetime of the structure always lead to a k^{-2} spectrum. Gilbert supposes that this result can be generalized to the 3D case of stretched spiral vortices, where a $k^{-5/3}$ should emerge after time averaging. Such a behaviour has been obtained and physically interpreted by Pullin *et al* [10] for the single spiral model which was used to perform computations presented in this section.

5.1. Evolution of the cumulative spectra

The experimental cumulative spectrum represents the averaged contribution of the vortex burst between $t = 0$ and t and is expected to be an equivalent to the cumulative spectrum in the numerical case. In both cases, we calculate the evolution of the cumulative spectrum slope, $p_{c,num}$ numerically and $p_{c,exp}$ experimentally, as time increases. Experimentally, $p_{c,exp}$ is obtained by fitting $E^c(k,t)$ with k^p using the range $1/\Delta r \leq k \leq k_M$ when $\Delta r \leq k_m^{-1}$ and in the whole inertial range when $\Delta r > k_m^{-1}$. Numerically, $p_{c,num}$ is computed using the whole inertial range ($1\,\mathrm{cm}^{-1} \leq k \leq 5\,\mathrm{cm}^{-1}$). Figure 9 shows the cumulative spectra $E^c(k,t)$ as a function of k numerically obtained for increasing t values. The spectral slope (inset of figure 9) is found to vary from a value close to -2 and to progressively reach $-5/3$ for $t = t_2 - t_1 = T_v$. This shows, as expected, that the $k^{-5/3}$ law results from time averaging over the vortex lifetime. Figure 10 is the experimental equivalent of figure 9. In this case, the spectral slope $p_{c,exp}$ (inset

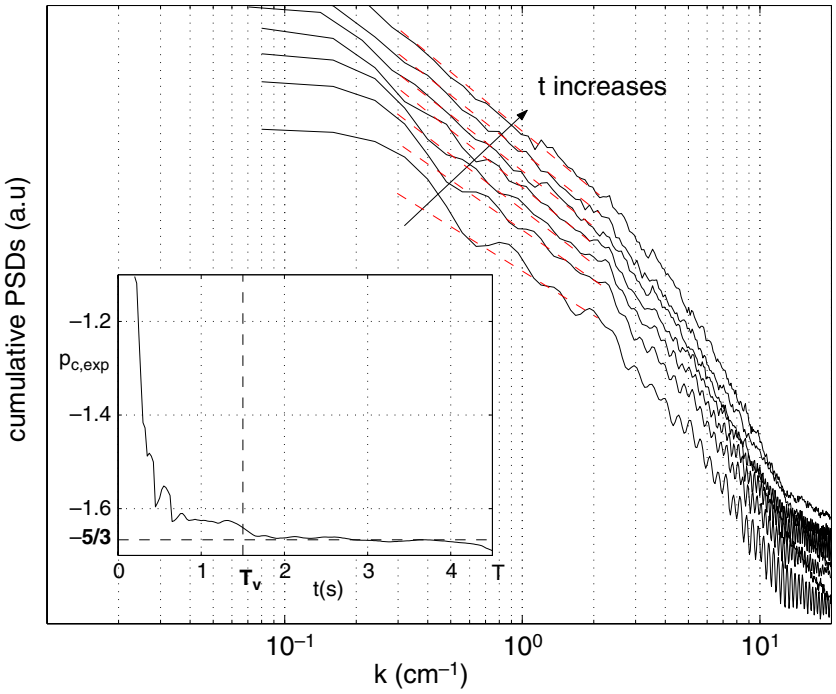

Figure 10. Experimental cumulative spectra $E^c(k,t) \simeq e_{\Delta t}(k,0)$ for increasing t values ($t = 0.25$, 0.34, 0.43, 0.61, 1.1, 1.5 and 4.5 s) (the fit in k^p is indicated by red dotted lines). The inset shows the variation of the k slope $p_{c,exp}$ versus t; see also animation 5.

in figure 10) is found to decrease from a value close to -1 for small times and it reaches the $-5/3$ value at T_v, and thereafter remains constant. To provide a more communicative representation of this result, animation 5 shows a time-evolving representation of the spectral slope and the corresponding temporal window plotted against the visualization of the flow.

From figures 9 and 10 we can conclude that both experimental and numerical processes of turbulent cascade build-up result from a temporal evolution of the spectra, whose averaging leads to a $k^{-5/3}$ behaviour. We can also confirm in both cases that the whole spectrum is built in a time $T_v = 1.5$ s.

The initial values of the spectral slope, -2 for Lundgren's spiral and -1 experimentally, can be attributed to the difference in the initial conditions: a vortex sheet-like structure in numerical calculations and probably a distribution of vorticity patches close to vortex tubes in the experiments.

5.2. Evolution of the instantaneous spectra

Figure 11 shows the instantaneous spectra $e(k,t)$ as a function of k numerically obtained for various times t. The evolution of the energy spectrum is in agreement with [11, 25] and shows a similar behaviour to the one predicted by Gilbert [26] for 2D spiral vortices. The instantaneous numerical spectra are characterized in the inertial range by two regions, a region $k < k_c(t)$ with a k^{-1} 'tube-like spectrum' and a region $k > k_c(t)$ with a k^{-2} 'sheet-like spectrum'. For the initial times, the spectrum is dominated by the k^{-2} region, as time increases, $k_c(t)$ increases until a near k^{-1} spectrum invades the whole inertial range. Consequently, the instantaneous spectra

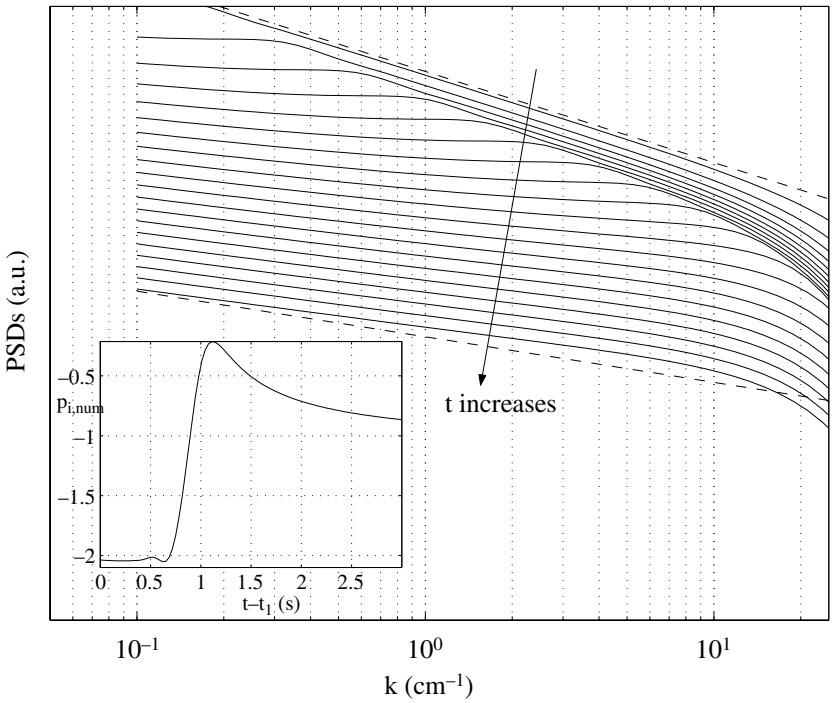

Figure 11. Numerical instantaneous spectra $e(k,t)$ for increasing t (time spacing is equal to 0.16 s) for $a = 1.55\,\mathrm{s}^{-1}$, $\alpha = 1395$ and $Re = 4000$. Spectra have been calculated from $t_1 \simeq 0.25$ to 3 s, with $t_2 \simeq 1.75$ s. The inset shows the instantaneous slope $p_{i,num}$ as a function of time (the origin corresponds to t_1).

slope $p_{i,num}$, computed using the inertial range ($k_m \simeq 1\,\mathrm{cm}^{-1} \ll k \ll k_M \simeq 5\,\mathrm{cm}^{-1}$), shows a transition from a value close to -2 to a value close to -1 (inset in figure 11). The evolution in the spectral space is the consequence of the roll-up of the spiral arm in the physical space (see figure 6). The thick vorticity layer presents for $t = t_1$ gives the initial k^{-2} contribution in the instantaneous spectrum. As the vorticity layer rolls-up and is simultaneously subjected to a lateral contraction, the spiral arm diffused in a vortex core. In the spectral space, this results in the transition to the k^{-1} spectrum.

The quasi-instantaneous spectrum $e_{\Delta t}(k,t)$, defined for small Δt, is an experimental equivalent to the instantaneous numerical spectrum. Figure 12 shows the time evolution of the quasi-instantaneous spectrum slope $p_{i,exp}$ for $\Delta r = 1.6$, 2 and 2.5 cm. As for the cumulative spectrum, an animation (animation 6) showing the evolution of the spectrum slope for $\Delta r = 1.6$ cm against a visualization of the flow is provided.

It can be seen that $p_{i,exp}$ varies from a value close to -1 to a value close to -2 when time increases from 0 to T_v, suggesting that the initial nonaxisymmetric vorticity field has a tube-like structure, which evolves with time into sheet-like structures. These tube-like structures result from the vortex burst (figure 2(c)). The transition, inverted compared with the numerical computation, may therefore be interpreted as a consequence of the difference in the initial nonaxisymmetric vorticity field, the instantaneous spectral slope being dependent on the type of vorticity that is wound up [26].

However, we do not observe experimentally two regions in the quasi-instantaneous spectra as in the numerical case. This can be due to a less resolved k-space in the post-processing. Further work is in progress to study such a possible transition.

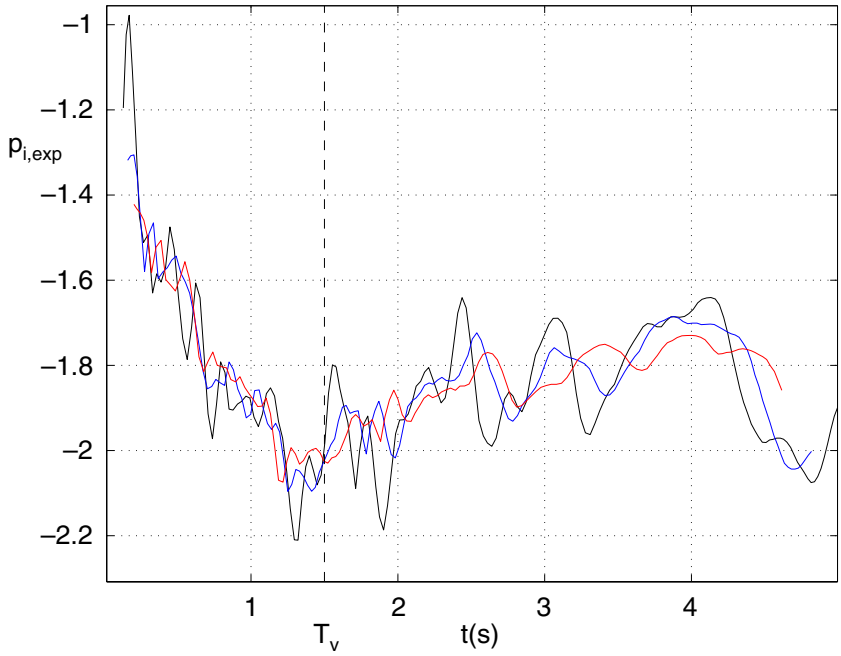

Figure 12. k-slope $p_{i,exp}$ of the quasi-instantaneous velocity PSDs as a function of time (quasi-instantaneous mean velocity PSD $e_{\Delta t}(k,t)$ averaged over a small Δt). To obtain a consistent representation, we have chosen a constant Δr for each curve: $\Delta r = 1.6$ cm (black); $\Delta r = 2$ cm (blue); $\Delta r = 2.5$ cm (red); see also animation 6.

6. Conclusion

We have presented an experiment where a stretched vortex is experiencing quasi-periodical turbulent bursts inside a laminar flow environment. It has been shown that the velocity fluctuations resulting from the bursts are responsible for the build-up of a turbulent $k^{-5/3}$ spectrum. Benefiting from the quasi-periodicity of the bursts, we have developed a data post-processing to characterize the build-up of the turbulent spectrum with time. This analysis has been particularly motivated by an existing theoretical framework for the energy transfer in that type of structure, notably the Lundgren mechanism.

To compare this mechanism with our experiment, we have performed numerical calculations according to Pullin *et al* [10, 23] for a particular solution of the Lundgren model. The results show that our experimental structure shares some common features with the theoretical structure proposed by Lundgren. In both cases, the instantaneous spectra varies with time while averaging over the lifetime of the structure results in a $k^{-5/3}$ spectrum. In addition, both the lifetime of the structure and the inertial range compare well. Finally, PIV measurements during the burst show a partial roll-up of a spiral structure qualitatively similar to the roll-up of the spiral arm in the numerical computation.

Future studies may address the following: first, PIV acquisitions synchronized to the probe acquisition will allow one to study more precisely the temporal evolution of the spectrum; and secondly, a numerical study of a Lundgren vortex with an initial condition closer to the experimental one, for instance a vorticity patch should allow a better comparison with the experiment. Work is in progress in these two directions.

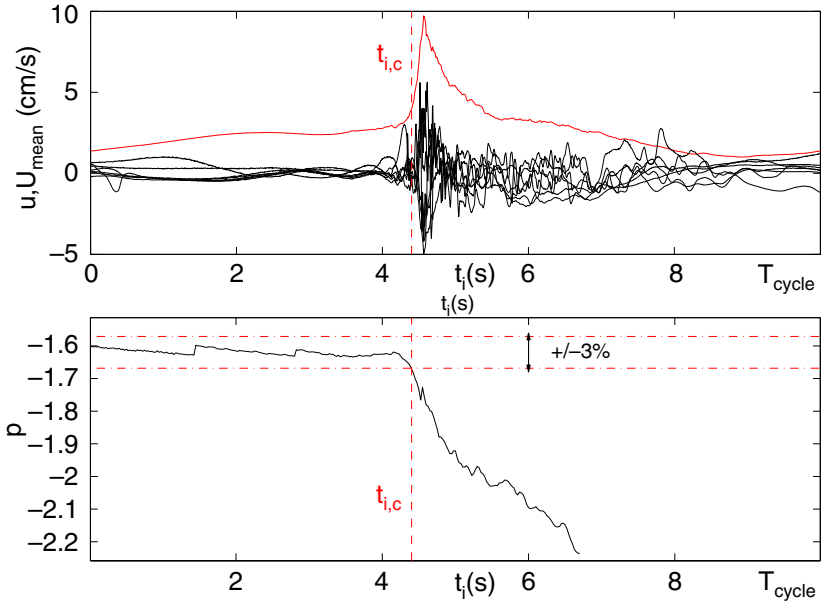

Figure A.1. Determination of $t_{i,c}$. Upper panel: velocity signal U_{mean} (red), u_n (black); lower panel: $p(t_i)$, slope of the experimental spectrum $e_{(T_{cycle}-t_i)}(k, t_i)$.

Appendix

In section 2.3, we have denoted by $\{t_n\}$ the inset of the turbulent part on each cycle. These initial times are defined as the times where the $k^{-5/3}$ turbulent spectrum starts to build up. To determine $\{t_n\}$ experimentally, we use the following procedure: in a first step, we define an arbitrary set of times $\{t_{0,n}\}$ as described in section 2.3 (in figure A.1, they are indicated as the origin of time). Then, we compute the averaged spectra $e_{(T_{cycle}-t_i)}(k, t_i)$ over the signals:

$$u_n(t_i \to T_{cycle}) = u_n\left(r = 0 \to r = \int_{t_i}^{T_{cycle}} U_{mean}(t')\,\mathrm{d}t'\right) \tag{A.1}$$

for increasing values of t_i, starting from $t_i = 0$. As expected, the first averaged spectrum $e_{T_{cycle}}(k, 0)$ has a spectral slope ($p(0) = -1.61$) in the inertial range very close to $-5/3$. Indeed, in that case, $e_{T_{cycle}}(k, 0) = E^c(k, T_{cycle}) \simeq E(k)$. When t_i increases, the parts of the velocity signals from $\{t_{0,n}\}$ to $\{t_{0,n} + t_i\}$ are suppressed. If these parts do not contribute to the turbulent cascade build-up, no influence on the spectra slope is expected. In contrast, if these parts contain information necessary to the cascade build-up process, the spectral slope is expected to depart from $-5/3$. Therefore, the initial time of the turbulent cascade build-up is the critical time $t_{i,c}$ for which the spectrum slope starts to diverge from $-5/3$. To determine $t_{i,c}$, we apply the following criterion: we consider that $t_{i,c}$ is reached when a significative divergence (=3%) between the spectra slope $p(t_i)$ and the mean value of the spectra slope, computed between $t_i = 0$ and $t_i = t_{i,c}$, is observed:

$$\left| p(t_{i,c}) - 1/t_{i,c} \int_0^{t_{i,c}} p(t_i)\,\mathrm{d}t_i \right| = 3\%. \tag{A.2}$$

We obtain $t_{i,c} = 4.4\,\mathrm{s}$ with the set of initial times $\{t_{0,n}\}$ chosen as in figure A.1. The new set of initial times $\{t_n\}$ are defined as $\{t_n = t_{0,n} + t_{i,c}\}$ and the final times as $\{t_n + T\}$.

References

[1] Douady S, Couder Y and Brachet M E 1991 Direct observation of the intermittency of intense vorticity filaments in turbulence *Phys. Rev. Lett.* **67** 983

[2] Siggia E D 1981 Numerical study of small-scale intermittency in 3-dimensional turbulence *J. Fluid. Mech.* **107** 375

[3] Lundgren T S 1982 Strained spiral vortex model for tubulent fine structures *Phys. Fluids* **25** 2193

[4] Townsend A A 1951 On the fine-scale structure of turbulence *Proc. R. Soc.* A **208** 534

[5] Tennekes H 1968 Simple model for small-scale structure of turbulence *Phys. Fluids* **11** 669

[6] Corrsin S 1962 Turbulent dissipation fluctuations *Phys. Fluids* **5** 1301

[7] Pullin D I and Saffman P G 1998 Vortex dyanmics in Turbulence *Ann. Rev. Fluid Mech.* **30** 31

[8] Kolmogorov A N 1941 Local structure of turbulence in an incompressible liquid for very large Reynolds numbers *C.R. Akad. Sci. SSSR* **30** 301

[9] Lundgren T S 1993 A small-scale turbulence model *Phys. Fluids* A **5** 1472

[10] Pullin D I, Buntine J D and Saffman P G 1994 On the spectrum of a stretched spiral vortex *Phys. Fluids* **6** 3010

[11] Voelkl T, Pullin D I and Chan D C 2000 A physical-space version of the stretched-vortex subgrid-stress model for large-eddy simulation *Phys. Fluids* **12** 1810

[12] Schwarz K W 1990 Evidence for organized small-scale structure in fully-developed turbulence *Phys. Rev. Lett.* **64** 415

[13] Kida S and Miura H 2000 Double spirals around a tubular vortex in turbulence *J. Phys. Soc. Japan* **69** 3466

[14] Cuypers Y, Maurel A and Petitjeans P 2003 Vortex burst as a source of turbulence *Phys. Rev. Lett.* **91** 194502

[15] Manneville S, Robres J H, Maurel A, Petitjeans P and Fink M 1999 Vortex dynamics investigation using an acoustic technique *Phys. Fluids* **11** 3380

[16] Petitjeans P, Wesfreid J E and Attiach J C 1997 Vortex stretching in a laminar boundary layer flow *Exp. Fluids* **22** 351

[17] Petitjeans P, Robres J H, Wesfreid J E and Kevlahan N 1998 Experimental evidence for a new type of stretched vortex *Eur. J. Mech. B: Fluids* **17** 549

[18] Rossi M, Bottausci F, Maurel A and Petitjeans P 2004 A non uniform stretched vortex *Phys. Rev. Lett.* **92** 54504

[19] Pinton J F and Labbe R 1994 Correction to the taylor hypothesis in swirling flows *J. Phys. II* **4** 1461

[20] Camussi R, Ciliberto S and Baudet C 1997 Experimental study of the evolution of a velocity perturbation in fully developed turbulence *Phys. Rev.* E **56** 6181

[21] Marcq P and Naert A 1998 A Langevin equation for the energy cascade in fully developed turbulence *Physica* D **124** 368

[22] Chanal O, Chabaud B, Castaing B and Hebral B 2000 Intermittency in a turbulent low temperature gaseous helium jet *Eur. Phys.* B **17** 309

[23] Pullin D I and Saffman P G 1993 On the Lundgren–Townsend model of turbulent fine structures *Phys. Fluids* A **5** 126

[24] Gilbert A D 1993 A cascade interpretation of Lundgren's stretched spiral vortex model *Phys. Fluids* **5** 2831

[25] Moffat H K 1993 Spiral structures in turbulent flows *Proc. IMA Conf.* ed M Farge, J C R Hunt and J C Vassilicos (London: Oxford University Press)

[26] Gilbert A D 1988 Spiral structures and spectra in two-dimensional turbulence *J. Fluid Mech.* **193** 475